UC Irvine

UC Irvine Previously Published Works

Title

Alternative Translation Initiation in Rat Brain Yields K2P2.1 Potassium Channels Permeable to Sodium

Permalink

https://escholarship.org/uc/item/9r54z0z0

Journal

Neuron, 58(6)

ISSN

0896-6273

Authors

Thomas, Dierk
Plant, Leigh D
Wilkens, Christina M
et al.

Publication Date

2008-06-01

DOI

10.1016/j.neuron.2008.04.016

Copyright Information

This work is made available under the terms of a Creative Commons Attribution License, availalbe at https://creativecommons.org/licenses/by/4.0/

Peer reviewed

eScholarship.org Powered by the California Digital Library
University of California

NIH Public Access
Author Manuscript
Neuron. Author manuscript; available in PMC 2009 June 26.

Published in final edited form as:
Neuron. 2008 June 26; 58(6): 859–870. doi:10.1016/j.neuron.2008.04.016.

Alternative translation initiation in rat brain yields $K_{2P}2.1$ potassium channels permeable to sodium

Dierk Thomas, **Leigh D. Plant**, **Christina M. Wilkens**, **Zoe A. McCrossan**, and **Steve A. N. Goldstein**

Department of Pediatrics and Institute for Molecular Pediatric Sciences, Pritzker School of Medicine, University of Chicago, 5721 S. Maryland Avenue, Chicago, IL 60637 USA

Abstract

K_{2P} channels mediate potassium background currents essential to central nervous system function, controlling excitability by stabilizing membrane potential below firing threshold and expediting repolarization. Here, we show that alternative translation initiation (ATI) regulates function of $K_{2P}2.1$ (TREK-1) via a novel strategy. Full length $K_{2P}2.1$ and an isoform lacking the first 56 residues of the intracellular N-terminus ($K_{2P}2.1$ Δ1-56) are produced differentially in a regional and developmental manner in the rat central nervous system, the latter passing sodium under physiological conditions leading to membrane depolarization. Control of ion selectivity via ATI is proposed to be a natural, epigenetic mechanism for spatial and temporal regulation of neuronal excitability.

Keywords

TREK-1; potassium channel; sodium; ATI; rat brain; central nervous system; leak; background; resting potential

Introduction

Over the past decade, a superfamily of *KCNK* genes encoding the two-P-domain potassium (K_{2P}) channels (now with 15 mammalian members) has been cloned. Their functional analysis has established unequivocally that leak currents are mediated by dedicated portals and do not accrue as a by-product of pathways devoted to other functions (Ketchum et al., 1995; Goldstein et al., 1996; Goldstein et al., 2001; Goldstein et al., 2005). K_{2P} channels are recognized as highly-regulated pores that stabilize membrane potential of excitable cells below firing threshold and expedite repolarization. Because membrane potential is fundamental to neuronal activity, leak current regulation is a primary and dynamic mechanism for control of cellular excitability. K_{2P} channels are identified by a unique structure of two pore-forming loop domains in each subunit. The channels assemble from 2 subunits to form a single ion conduction pathway (Lopes et al., 2001). As expected for key regulators of excitability, K_{2P} channels are under tight control from a multitude of chemical and physical factors (Goldstein et al., 2005).

Correspondence should be addressed to: sangoldstein@uchicago.edu.

Competing interests statement The authors declare that they have no competing financial interests.

Publisher's Disclaimer: This is a PDF file of an unedited manuscript that has been accepted for publication. As a service to our customers we are providing this early version of the manuscript. The manuscript will undergo copyediting, typesetting, and review of the resulting proof before it is published in its final citable form. Please note that during the production process errors may be discovered which could affect the content, and all legal disclaimers that apply to the journal pertain.

NIH-PA Author Manuscript
NIH-PA Author Manuscript
NIH-PA Author Manuscript

NIH-PA Author Manuscript

NIH-PA Author Manuscript

NIH-PA Author Manuscript

Expressed robustly in the central nervous system (CNS), especially in the hippocampus, the prefrontal cortex and the hypothalamus, $K_{2P}2.1$ (TREK-1) channels are implicated in physiological processes including, depression, neuromodulation, neuroprotection and sensation of mechanical stress and temperature (Maingret et al., 2000; Heurteaux et al., 2006; Honore et al., 2006). $K_{2P}2.1$ channels are regulated by a plethora of stimuli including lipids, mechanical stretch, neurotransmitters, and activators of G-protein coupled receptors and intracellular second messengers (Goldstein et al., 2005). In addition, $K_{2P}2.1$ leak currents are targets for compounds in clinical use, such as, neuroprotective drugs, antidepressants and volatile and local anesthetics (Kindler et al., 1999; Patel et al., 1999; Duprat et al., 2000; Kennard et al., 2005). Single $K_{2P}2.1$ channels show dynamic protein kinase A-dependent versatility: native hippocampal and cloned $K_{2P}2.1$ channels transform in reversible fashion from potassium-selective leak conductances to strictly voltage-dependent channels (Bockenhauer et al., 2001).

Here, full length $K_{2P}2.1$ and a truncated isoform lacking 56 N-terminal residues (Δ1-56) are shown to be differentially expressed across the rat CNS. Expression of Δ1-56 leads to decreased macroscopic outward potassium currents and plasma membrane depolarization, effects that are explained by decreased open probability and altered selectivity allowing sodium permeation. Δ1-56 subunits form homomeric channels and assemble with full-length subunits. Alternative translation initiation (ATI) of $K_{2P}2.1$ is found to be a natural strategy to alter ion channel function and neuronal excitability.

RESULTS

ATI yields full-length and truncated $K_{2P}2.1$ subunits in rat CNS and *in vitro*

Rat $K_{2P}2.1$ subunits are predicted from the *KCNK2* gene sequence to have 426 amino acids and a molecular mass of 47 kDa. Analysis of native $K_{2P}2.1$ protein purified from total rat brain with antibodies to the channel C-terminus revealed an unexpected finding: a smaller variant of 41 kDa in addition to the predicted 47 kDa protein, Figure 1A. To confirm the identity of the lower band as $K_{2P}2.1$, it was visualized with antibodies to a different epitope on the C-terminus and shown to be absent on pre-incubation of anti- $K_{2P}2.1$ antibodies with recombinant channel protein or when isolation was performed with non-immune IgG, Figure 1A. The smaller and larger $K_{2P}2.1$ proteins were revealed to be expressed at different ratios across adult rat CNS, with high relative expression of the 41 kDa isoform in whole brain, cortex, and hypothalamus, and low levels in cerebellum and spinal cord, Figure 1B. In contrast, neonatal rat cerebellum harboured a significant amount of the short variant that was suppressed on maturation, while cortical expression patterns were similar in neonates and adults, Figure 1C. Based on regional differences in adults and variation with developmental stage, we hypothesized that the 41 kDa isoform might confer functional differences on tissues of high relative expression and so merited further investigation.

To elucidate the nature of the lower molecular weight variant, *KCNK2* cDNA was expressed in COS-7 African Green Monkey fibroblasts. Two bands at 41 kDa and 47 kDa were detected by Western blot analysis with antibodies to $K_{2P}2.1$ (Figure 1D) and these were identified by tandem mass spectrometry (MS/MS) and direct amino-terminal Edman sequencing (Figures S1 and S2A) to be full-length $K_{2P}2.1$ protein (47 kDa) and a truncated variant starting at position M57 and therefore lacking N-terminal residues 1-56 (41 kDa; $K_{2P}2.1\Delta1$-56), Figure 1E. In accord with these identifications, Western blot of $K_{2P}2.1$ proteins purified from rat brain revealed both the 41 and 47 kDa isoforms with antibodies to the C-terminus but only the 47 kDa product with antibodies to the channel N-terminus, Figure 1F.

Examination of the $K_{2P}2.1$ coding sequence revealed the Kozak translation initiation context (Kozak, 1991) at M1 to be sub-optimal compared to the downstream translation context at M57

NIH-PA Author Manuscript

NIH-PA Author Manuscript

NIH-PA Author Manuscript

due to a purine at position -3 in the latter case (*gca ugc cuc AUG c* and *auu aau guu AUG a*, respectively). These sequences are shared in rat and human *KCNK2* genes (Figure S2B) and rationalize the basis for production of Δ1-56 channels in rat CNS and tissue culture cells as ready downstream translation initiation due to "leaky" ribosome scanning of K_{2P}2.1 mRNA. This recognized mechanism to create protein diversity in prokaryotes has recently been observed in eukaryotic cells (Fernandez et al., 2003; Touriol et al., 2003; Cai et al., 2006). Consistent with this, expression in COS-7 cells of the K_{2P}2.1 open reading frame employing an optimized initiation sequence (Experimental Methods) produced relatively less of the 41 kDa product (Figure 1D, H) than observed in whole rat brain preparations, Figure 1F.

Full-length and Δ1-56 channel subunits co-assemble

To determine the properties of both K_{2P}2.1 isoforms, two mutant *KCNK2* genes were synthesized. One gene yields only full length channel due to mutation of the downstream methionine to isoleucine producing M57I-K_{2P}2.1 channels (M57I); the second was designed to produce only the truncated variant Δ1-56-K_{2P}2.1 (Δ1-56) because codons for the first 56 residues are deleted. The predicted topology of both isoforms includes cytoplasmic N- and C-termini, 4 transmembrane segments and 2 pore-forming P loops. These channels were produced with a C-terminal epitope tag (1d4) to allow ready visualization on heterologous expression; as expected, the M57I gene in *Xenopus laevis* oocytes produced only the 47 kDa channel and Δ1-56 only the 41 kDa isoform (Figure 1G). While the relative amounts of 41 to 47 kDa produced from the wild type gene with an optimized initiation motif in COS-7 cells (Figure 1D) resembled protein expression patterns found in rat cerebellum and spinal cord (Figure 1B), cortex and hypothalamus were better approximated by expression of equimolar amounts of M57I and Δ1-56 subunits, Figure 1G and 1B, respectively.

Arguing against the idea that Δ1-56 was produced via degradation of full-length channel rather than ATI, low molecular mass bands were not visualized on expression of M57I in oocytes (Figure 1G) or COS-7 cells even after affinity purification with antibody to the C-terminus (Figure S2C). Additionally, the channel N-terminus contains no known selective protease cut sites and neither control oocytes (not shown) nor COS-7 cells transfected with empty vector showed K_{2P}2.1 signals (Figure 1D).

Consistent with stable association of full-length and truncated K_{2P}2.1 isoforms, Δ1-56 was not isolated by antibodies to the "missing" 56 N-terminal residues when this protein was expressed alone but Δ1-56 was co-purified with full length subunits when the two were co-expressed in oocytes or in COS-7 cells (Figures 1G and 1H).

Δ1-56 yields smaller outward currents and membrane depolarization

To assess the effect of ATI on K_{2P}2.1 biophysical function, the channels were studied in oocytes. Compared to cells expressing wild type transcript, M57I full length subunits yielded potassium currents of slightly greater magnitude whereas Δ1-56 subunits alone and Δ1-56 expressed at equal cRNA levels with M57I had reduced outward currents that remained distinguishable from basal endogenous currents, Figure 2A-E.

Isoform-dependent effects on current magnitude were accompanied by changes in resting membrane potential, Figure 2F. Oocytes expressing M57I had a resting potential of -78.2 ± 0.4 mV (n = 21), close to the predicted reversal potential for potassium ions (-81.2 mV). In contrast, Δ1-56 channel expression depolarized the membrane to -56.1 ± 1.7 mV under the same conditions (n = 21). Equimolar mixtures of M57I and Δ1-56 cRNA led to an intermediate value of -72.0 ± 0.9 mV (n = 21) whereas wild type K_{2P}2.1 with an optimized initiation sequence was not distinguishable from M57I.

NIH-PA Author Manuscript

NIH-PA Author Manuscript

NIH-PA Author Manuscript

Δ1-56 channels have wild type membrane expression

Small macroscopic currents can be associated in the first instance with failure of the protein to reach the plasma membrane. To investigate trafficking of $K_{2P}2.1$ isoforms, the proteins were studied as fusion products bearing C-terminal fluorescent tags for visualization in live Chinese Hamster Ovary (CHO) cells; Green Fluorescent Protein (GFP) was incorporated into wild type $K_{2P}2.1$ nucleotide sequence (WT); Cyan Fluorescent Protein (CFP) into M57I; and, Yellow Fluorescent Protein (YFP) into Δ1-56. All 3 constructs alone and M57I with Δ1-56 showed strong fluorescence at the CHO cell plasma membrane, Figure 3A.

Expression assessed by labeling oocyte surface proteins with a membrane-impermeant biotinylation reagent similarly demonstrated trafficking of M57I, Δ1-56 and M57I with Δ1-56 subunits to the cell surface, Figure 3B. As expected from functional assessment (Figure 2F), *K2P2* with an optimized initiation sequence yields little of the lower molecular weight subunit on expression in *Xenopus* oocytes. Outward currents recorded from the same oocytes that were later subjected to biochemical analysis demonstrated that whole cell Δ1-56 currents were 5.3-fold smaller than those passed by full-length M57I subunits ($p < 0.01$; $n = 3$) despite similar amounts of protein on the cell surface (M57I to Δ1-56 surface protein ratio was 1:0.82 ($p > 0.05$; $n = 3$), Figure 3C.

Δ1-56 channels show reduced open probability but larger unitary conductance

Reduced macroscopic currents despite normal surface expression must be due to either reduced open probability and/or smaller unitary conductance. To assess the mechanism for current reduction on expression of Δ1-56 subunits, single $K_{2P}2.1$ channels were recorded at −60 and 60 mV in inside-out patches excised from oocytes with symmetrical 150 mM KCl solutions, Figure 4A, B. Open probability of single M57I channels was found to be 6.4-fold greater than for Δ1-56 channels at +60 mV with values of 0.051 ± 0.016 ($n = 3$ patches) and 0.008 ± 0.002 ($n = 9$), respectively. At −60 mV, M57I channels showed a 6.6-fold higher open probability (0.046 ± 0.018, $n = 6$) than and Δ1-56 channels (0.007 ± 0.002, $n = 9$), Figure 4C. These values are best estimates because more than one channel in patches cannot be ruled out given such low open probability.

Changes in unitary currents did not appear to contribute to lower macroscopic Δ1-56 currents. Δ1-56 single channel conductance was ~30% larger than for M57I channels (83 ± 5 and 60 ± 4 pS at −60 mV, respectively), Figure 4D. Co-expression of Δ1-56 and M57I subunits yielded patches with low conductance channels, high conductance channels, and patches with both channel types; we speculate that both M57I and heteromeric channels have the lower conductance as this was seen more frequently in patches with a single channel (10 *versus* 5). Based upon these measurements, channels formed with M57I subunits would be expected to display ~4.8-fold larger macroscopic currents than Δ1-56 subunits, consistent with observation, Figure 3C. Despite the characteristic “flicker-burst” pattern of $K_{2P}2.1$ single channel openings (Figure 4A) that might make it difficult to discern variation in peak amplitude, concern is mitigated by invariance of measured peak currents at twice the filter frequency (5.6 kHz, not shown) and observation that Δ1-56 channels have a smaller Po than M57I but a larger unitary conductance.

Δ1-56 channels are permeable to potassium and sodium

In addition to reduced outward currents, expression of Δ1-56 channels led to a depolarizing shift in resting membrane potential, Figure 2F. Because depolarization might be explained by passage of ions other than potassium through Δ1-56 channels, ion selectivity was assessed, first, with oocytes in whole-cell mode by variation of bath potassium via isotonic substitution with sodium. M57I channels displayed the expected attributes of a potassium-selective leak (Figure 5A and 5B) operating as a voltage-independent portal showing outward rectification.

NIH-PA Author Manuscript

NIH-PA Author Manuscript

NIH-PA Author Manuscript

This manifests in a linear current-voltage relationship when potassium concentrations across the membrane approach symmetry and yields greater outward than inward currents under physiological ionic conditions of low external potassium. With 4 mM bath potassium, M57I inward currents were small even at hyperpolarized voltages and the reversal potential (E_{rev}) was −80 ± 1 mV (n = 16) near E_K. Further, as bath potassium was substituted with sodium, E_{rev} shifted in nearly perfect agreement with values predicted by the Nernst relationship (Figure 5A) indicating high selectivity of M57I channels for potassium over sodium.

In contrast, Δ1-56 channels with 4 mM bath potassium displayed significant inward currents and showed a reversal potential of −61 ± 1 mV, Figure 5A (n = 16). As external potassium was varied, a sub-Nernstian relationship between E_{rev} and potassium was revealed, consistent with permeability for the substituting ion, sodium. Co-expression of M57I and Δ1-56 produced a depolarizing change in reversal potential (−76 ± 1 mV; n = 16, Figure S3) less than the average of the two channel types suggesting heteromeric channels are more selective than Δ1-56 channels.

The hypothesis that inward currents and reversal potential changes result from sodium flux via Δ1-56 was further supported by study of whole-cell currents in the presence of a single monovalent cation in the bath: potassium, sodium or the impermeant cation, N-methyl-d-glucamine (NMG). Whereas M57I and Δ1-56 channels both pass potassium and do not pass NMG, significant inward sodium currents were observed only with the truncated channels, Figure 5B.

Δ1-56 and full length channels vary in permeability sequence and AMFE

Whole-cell reversal potential measurements with M57I channels revealed relative permeability similar to an Eisenman type IV series ($K^+ > Rb^+ > NH_4^+ > Cs^+ > Li^+ > Na^+$; Tables 1 and 2) with low relative permeability for sodium compared to potassium, $P_{Na}/P_K \sim 0.02$. Conversely, Δ1-56 channels were not as highly selective for potassium over sodium ($P_{Na}/P_K \sim 0.18$) and displaying permeability similar to an Eisenman type V sequence ($K^+ > Rb^+ > NH_4^+ > Na^+ > Li^+ > Cs^+$; Table 1 and 2). Channel populations formed with equal mixtures of M57I and Δ1-56 cRNAs exhibited an intermediate relative permeability for sodium (P_{Na}/P_K of 0.06s).

Pores that allow multi-ion occupancy can demonstrate an anomalous mole fraction effect (AMFE) in mixtures of two permeant ions. Channels that hold a single ion at a time or pass one ion type show currents that rise monotonically with increased mole fraction of permeant ion, even in mixed solutions, as seen with full-length M57I channels in solutions where potassium levels are increased by substitution for sodium, Figure 5C and Figure S4. In contrast, Δ1-56 channels displayed a biphasic course with a minimum near 3 mM with increasing potassium concentration. This AMFE is consistent with permeation of potassium and sodium, competition of the two ions for simultaneous occupancy of the conduction pathway, and decreased current due to potassium block of sodium current as bath potassium increases from nominally zero to 3 mM.

Decreased length of the N-terminus allows sodium flux

To investigate the requirements for altered sodium permeability with N-terminal truncation, M57I channels were compared to mutants where progressive portions of the N-terminus were deleted and relative permeability assessed via reversal potential measurements, Figure 6 and Table S1. High selectivity for potassium over sodium was maintained when the N-terminus was shortened by 16 residues (isolate 2), an isoform found *in vivo* due to mRNA splice variation (Fink et al., 1996). Indeed, potassium selectivity was maintained even on removal of 52 residues (isolate 7). Although further deletion of amino acids I54, N55, and V56 resulted in progressive loss of potassium selectivity (isolates 8-10), altering these 3 residues individually

NIH-PA Author Manuscript

NIH-PA Author Manuscript

NIH-PA Author Manuscript

or as a group to alanine in an M57I backbone yielded high selectivity for potassium as observed with full-length channels. This suggested that the N-terminus required a critical length rather than a specific motif to maintain potassium selectivity.

Subunits linked in series

To further interrogate the trafficking and function of homomeric and mixed subunit complexes 4 tandem constructs were studied: M57I–M57I, Δ1-56– Δ1-56, M57– Δ1-56, and Δ1-56–M57I. All tandem constructs gave rise to ionic currents, suggesting naturally-heteromeric channels can reach the plasma membrane and function. Dimeric constructs lacking residues 1-56 from the first channel subunit (i.e., Δ1-56– Δ1-56 and Δ1-56–M57I) showed reduced macroscopic currents, depolarized resting membrane potential, and less selectivity for potassium over sodium compared to those with a full length N-termini (M57I–M57I and M57I– Δ1-56), although changes were less than for channels composed of single Δ1-56 subunits, Table S2 and Figure S5.

Thus, evaluation of tandem channels and the inferred behavior of heteromeric channels suggest that the N-terminus influences single channel conductance (Figure 4D), sodium permeability and, thereby, resting membrane potential (Figure S3), that tandem linkage mimics the effects of a longer N-terminus, and that tandems and mixed complexes are more like 47 kDa and M57I channels rather than Δ1-56 channels.

Δ1-56 channels depolarize rat hippocampal neurons

To directly investigate the effects of Δ1-56 channel subunits on excitability in a native environment, rat hippocampal neurons were studied in primary culture; please note that these experiments did not report on ATI in tissue culture because they were designed for maximal subunit expression in a neuronal microenvironment using optimized initiation sequences (Experimental Methods) that diminish ATI with the wild type $K_{2P}2.1$ open reading frame (Figure 1H) or explicitly prevent it via encoding of M57I or Δ1-56 subunits. cDNA encoding $K_{2P}2.1$ wild type, M57I, Δ1-56 or an equimolar mixture of the two isoforms were expressed and cells assessed by voltage-clamp and current-clamp in whole-cell mode (Table 3, Figure S6). Voltage-clamp recordings demonstrated that relative macroscopic current levels for the isoforms (normalized to empty vector current amplitudes) were like those in oocytes, M57I > WT > M57I + Δ1-56 > Δ1-56. Two measures of excitability were considered: resting membrane potential and membrane input resistance (a measure of change in voltage on current injection reflecting open channels). Under baseline conditions (E_K −90 mV), the neurons had a mean membrane potential of −62.6 ± 0.7 mV and a mean input resistance of 91.1 ± 1.0 MΩ (n = 10). Neurons over-expressing M57I channels were hyperpolarized toward E_K to −75.4 ± 0.6 mV and exhibited a mean relative input resistance of 0.86 ± 0.02 (n = 10). Conversely, membrane potential on expression of Δ1-56 channels was depolarized to −55.9 ± 1.0 mV with a relative input resistance of 0.96 ± 0.01 (n = 9). On co-expression of the 2 isoforms, membrane potential was intermediate at −71.0 ± 0.5 mV with relative input resistance of 0.87 ± 0.02 (n = 7). Cells expressing $K_{2P}2.1$ wild type channels also displayed intermediate values with membrane potential of -74.1 ± 0.7 mV and relative input resistance of 0.92 ± 0.01 (n = 4).

DISCUSSION

K_{2P} potassium channels stabilize membranes of excitable cells at hyperpolarized potentials below the threshold for action potential firing. Since the gradient of ions across membranes is set by ion pump activity and does not change appreciably during action potentials, membrane potential is primarily dependent on baseline permeability. Resting potential is often close to E_K because more potassium channels are open at rest than pathways for other ions. Increased sodium permeability modifies excitable activity by depolarizing cells; small increases shift

NIH-PA Author Manuscript

NIH-PA Author Manuscript

NIH-PA Author Manuscript

R_M toward threshold leading to more ready firing; moderate depolarizations can inactivate voltage-dependent channels that initiate firing leading to hypo-excitability; excessive sodium flux leads to apoptosis (Kofuji et al., 1996). Here, we identify alternative mRNA translation initiation as an unexpected natural mechanism to alter excitability in the CNS. ATI serves to regulate K_{2P}2.1 function by producing 2 subunit forms at various levels in different CNS regions and times in development that vary in activity level and selectivity for potassium over sodium. This leads to depolarizing shifts in resting membrane potential under physiological ionic conditions in *Xenopus* oocytes or hippocampal neurons over-expressing the subunits in primary culture.

In rat CNS, *KCNK2* expression is found to produce two K_{2P}2.1 channel variants of 47 and 41 kDa that were identified to be full-length and truncated K_{2P}2.1 polypeptides, respectively. The expression ratio of the two isoforms is differential across the CNS with high relative expression of the short form in cerebral cortex and hypothalamus and low levels in cerebellum and spinal cord, Figure 1. Analysis of *KCNK2* genomic DNA and cDNA sequences does not provide evidence for alternative RNA splicing at this position. Rather, the isoforms arise from alternative initiation of mRNA translation beginning at either of two initiation codons, M1 and M57, Figure S1.

ATI is recognized to contribute to protein diversity by expression of two or more proteins from a single mRNA (Cai et al., 2006). Translation initiation of most eukaryotic mRNAs follows a linear scanning mechanism where the 40S ribosome is recruited to the 5’ cap structure of the mRNA followed by downstream movement until an initiation codon is encountered (Kozak, 1999). In these cases, the translation initiation site is the first cap-proximal start codon for methionine (AUG). However, if the first AUG is within a weak sequence context (Kozak, 1991) it may be used inefficiently and some ribosomes read through the site without recognition, resulting in “leaky scanning” and translation initiation at a downstream position. A purine at -3 and guanine at +4 with respect to an AUG make the largest contribution to initiation efficiency and neither is present at M1 in K_{2P}2.1. Thus, leaky scanning yields generation of Δ1-56 channels via initiation at M57, an AUG bearing a -3 purine. Functional analyses of cloned full-length and truncated channel proteins offered a physiological significance for this phenomenon.

Δ1-56 channels differ from full-length channels in their selectivity for potassium over sodium. Reversal potential measurements illustrate increased relative sodium permeability in Δ1-56 compared to those with full-length subunits, Table 1. Truncated channels display anomalous mole fraction behavior (Figure 5), consistent with a single pore that can simultaneously contain potassium and sodium ions (Ilan and Goldstein, 2001) and competition between the ions for occupancy in the conduction pathway (Korn and Ikeda, 1995). Under physiological ionic conditions, Δ1-56 channels depolarize resting membrane potential of oocytes by 22 mV and hippocampal neurons by 20 mV relative to cells expressing M57I full-length subunits (Figure S2 and Table 3). Decreased outward currents via Δ1-56 channels compared to M57I channels appear to result from reduced open probability (Figure 4), as their unitary conductance is larger (Figure 4) and surface expression intact, Figure 3; indeed, comparing surface and total cellular content suggests homomeric Δ1-56 channels are delivered more efficiently to the plasma membrane or turnover more slowly than those formed with M57I, Figure 3B.

The attributes of heteromeric channels were considered by study of linked tandem dimers (Table S2 and Figure S5) and co-expression of the 2 isoforms. Cautiously recognizing limits on interpretation because properties of linked Δ1-56 subunits were modified relative to channels of monomers and natural heteromers were studied in a sea of homomers, we suggest native M57I + Δ1-56 channels have mixed characteristics including M57I-like unitary conductance (Figure 4), lower open probability than M57I channels (Figure 2), and are less

NIH-PA Author Manuscript

NIH-PA Author Manuscript

NIH-PA Author Manuscript

selective for potassium than M57I channels but more discriminating than Δ1-56 channels (Table 2). Subunit recovery by immunoprecipitation was consistent with expectations for unbiased subunit synthesis and assembly (Figure S2).

The basis for ion selectivity

Despite opposing roles in cellular excitation, it is perhaps not a surprise that a potassium channel can be modified to pass sodium ions. Voltage-gated Kv2.1 channels (Korn and Ikeda, 1995), *Shaker* channels (Starkus et al., 1997) and Kv1.5 channels (Wang et al., 2000) pass sodium on removal of potassium and under normal ion conditions during transition from the open to inactivated state (Kiss et al., 1999). Indeed, sodium permeation is measured in small-conductance calcium-activated potassium channels (Shin et al., 2005), hyperpolarization-activated cyclic nucleotide-gated pacemaker channels (Macri et al., 2002), and with monovalent cation permeability ratios change on expression of the accessory subunit MinK with KCNQ1 to form cardiac I_{Ks} channels (Wollnik et al., 1997; Sesti and Goldstein, 1998). Potassium channels are selective due to pore sites that favor potassium over sodium and they conduct due to charge repulsion between ions in the transmembrane pathway (Neyton and Miller, 1988a; Neyton and Miller, 1988b; Doyle et al., 1998; Noskov et al., 2004). As K_{2P} channels have recognizable selectivity sequences and operate at macroscopic and single channel level like their voltage-gated brethren (Goldstein et al., 1996; Ilan and Goldstein, 2001; Zilberberg et al., 2001) we presume removal of 56 N-terminal residues, including 3 that precede the second start methionine and are critical (Figure 6), alters the structure of the ionic conduction pathway so it is more accommodating of sodium (Noskov et al., 2004; Shi et al., 2006).

ATI dynamically regulates function of other mammalian proteins

ATI is a known mechanism to create protein diversity in prokaryotes and has recently been recognized to function in eukaryotic cells (Touriol et al., 2003; Cai et al., 2006). Tissue-specific synthesis of proteins harboring different N-terminal domains from a single mRNA has been shown to alter subcellular localization and function of transcription and growth factors, cell cycle regulators, hormone receptors, and protein kinases. Ion channels, previously shown to be regulated by ATI in experimental cells (Fernandez et al., 2003), now join the inventory of mammalian proteins subject to ATI based on regional expression of distinct K_{2P}2.1 isoforms in rat central nervous system (Figure 1).

Emerging evidence suggests that ATI is a regulated process although the molecular control mechanisms are not yet understood. ATI of glucocorticoid and fibroblast growth factor 2 (FGF-2) receptors varies across tissues to yield functionally different isoforms important to their physiological function (Touriol et al., 2003; Lu and Cidlowski, 2005; Rhen and Cidlowski, 2005). Levels of FGF-2 isoforms vary *in vitro* with high cell density (Galy et al., 1999), heat shock and oxidative stress (Kevil et al., 1995; Vagner et al., 1996). Furthermore, ATI has been implicated in cancers including Burkitt's lymphoma, T cell acute lymphoblastic leukemia and retinoblastoma (Hann et al., 1988; Mellentin et al., 1989; Sánchez-Sánchez et al., 2006).

A molecular mechanism to adjust excitability

The findings suggest ATI plays a distinct role in CNS function that could not have been anticipated. K_{2P}2.1 channels are revealed as tunable mediators of membrane potential through changes in sodium permeability rather than simply potassium-selective leaks whose activity moves membrane potential toward E_K. Furthermore, ATI of K_{2P}2.1 channels represents another molecular basis for voltage-insensitive background sodium conductance along with a recently recognized neuronal channel, NALCN (Lu et al., 2007). The idea that various levels of the two K_{2P}2.1 isoforms influence normal physiology is supported by their effects in hippocampal neurons where Δ1-56 subunits induce depolarization toward firing threshold and

NIH-PA Author Manuscript

NIH-PA Author Manuscript

NIH-PA Author Manuscript

M57I subunits produce hyperpolarization (Table 3). In cortex and hypothalamus high relative expression of Δ1-56 subunits is predicted to favor depolarization whereas greater expression of full-length $K_{2P}2.1$ channels in cerebellum and spinal cord should lead to stabilization below firing threshold. As a role for voltage-independent leaks that resemble K_{2P} channels has been suggested in the pathogenesis of some forms of epilepsy (Heinemann et al., 1986), differential generation of $K_{2P}2.1$ isoforms may play a role in resistance or predisposition to seizures. The spatiotemporal influence of $K_{2P}2.1$ channels on neuronal excitation will depend on their relative contribution to establishing membrane potential among all pathways active at rest.

METHODS

Molecular biology

cDNA encoding the 426-amino-acid isolate of human $K_{2P}2.1$ ($hK_{2P}2.1$) used in this work (GenBank accession number EF165334) was amplified from a brain cDNA library (Clontech, Palo Alto, CA), inserted into pCR2.1-TOPO (Invitrogen, Carlsbad, CA) and subcloned into pMAX, a dual-purpose expression vector containing a CMV promoter for mammalian expression and a T7 promoter for cRNA synthesis, and containing a modified translation initiation sequence (GCC GCC ACC) preceding the first start codon. Mutations described in the text were made with a QuikChange Site-Directed Mutagenesis kit (Stratagene, La Jolla, CA). N-terminal truncations and introduction of C-terminal 1d4 epitope tags (RVPDGDPDETSQVAPA, following a proline linker) were achieved using PCR. Enhanced Green, Yellow and Cyan Fluorescent Protein (eGFP, eYFP, eCFP) sequences were amplified from pEGFP-C2, pEYFP-C1, and pECFP-C1 vectors (Clontech) and ligated to the C-terminus of $hK_{2P}2.1$, $hK_{2P}2.1$ Δ1-56, and M57I-$hK_{2P}2.1$, respectively. The region of rat $K_{2P}2.1$ ($rK_{2P}2.1$, accession number AF325671) encoding the C-terminal 68 amino acids was amplified by PCR and subcloned in-frame downstream of the sequence for glutathione S-transferase (GST) in the bacterial expression vector, pGEX6P-1 (GE Healthcare, Piscataway, NJ). Tandem dimer constructs (M57I-M57I, Δ1-56-Δ1-56, M57I-Δ1-56, Δ1-56-M57I) were generated by linking two respective $hK_{2P}2.1$ open reading frames within the pMAX expression vector. The short peptide linker (AAGASLSGA) contained both a unique restriction site (*Hind*III) and a nucleotide sequence allowing for DNA sequencing.

All cDNA constructs were confirmed by DNA sequencing. cRNAs were transcribed after vector linearization using T7 RNA polymerase and the mMessage mMachine kit (Ambion, Austin, TX). Transcripts were quantified by spectrophotometry and integrity assessed by agarose gel electrophoresis.

Purification of recombinant $rK_{2P}2.1$ and antibody production and purchase

Recombinant C-terminal $rK_{2P}2.1$ protein containing 68 amino acids (CT68) was produced in *Escherichia coli* BL-21(DE3) competent cells (EMD Biosciences, Darmstadt, Germany) lysed with a Microfluidizer (Microfluidics, Newton, MA) and purified by solubilization with 1% TRITON X-100 followed by cleavage from its GST fusion product with PreScission protease (GE Healthcare). The $rK_{2P}2.1$ C-terminus was subjected to SDS-PAGE, visualized with Coomassie blue and excised from the gel. To generate a different specific antibody, a synthetic 26 amino acid peptide (CT26 sequence: GNHNQELTPCRRTLSVNHLTSEREVL), corresponding to residues 371-396 of $rK_{2P}2.1$ and displaying 1 amino acid difference compared to $hK_{2P}2.1$, was synthesized by the W.M. Keck Biotechnology Resource Laboratory (New Haven, CT) and fused to keyhole limpet (*Megathura crenulata*) hemocyanin (KLH; Calbiochem, San Diego, CA). The $rK_{2P}2.1$ C-terminus and the CT26 peptide were injected into different rabbits (Pocono Rabbit Farm and Lab, Canadensis, PA). Immunoglobulin was purified using Protein A Sepharose beads (GE Healthcare), and specific antibody was affinity-purified on CT68 or CT26 peptide-loaded Affi-Gel 10 columns (Bio-Rad Laboratories,

NIH-PA Author Manuscript

NIH-PA Author Manuscript

NIH-PA Author Manuscript

Hercules, CA). No specific bands were detected in untransfected COS-7 cells or in cells expressing $K_{2P}2.1$ when probed with the preimmune sera (not shown).

Purchased polyclonal (p) or monoclonal (m) antibodies used include: 1d4 (m, developed in mouse; National Cell Culture Center, Minneapolis, MN), h$K_{2P}2.1$ (p, T6448, developed in rabbit using a peptide corresponding to the N-terminus; Sigma, Saint Louis, MO), $K_{2P}2.1$ (p, C-20, developed in goat using a peptide corresponding to the C-terminus; Santa Cruz Biotechnology, Santa Cruz, CA), $K_{2P}2.1$ (p, E-19, developed in goat using a different peptide corresponding to the C-terminus; Santa Cruz Biotechnology). All $K_{2P}2.1$ antibodies used recognize both human and rat $K_{2P}2.1$. Secondary antibodies raised in goat against the relevant species (rabbit, mouse) conjugated to Alexa-Fluor 680 or to IRDYE800CW were obtained from Invitrogen and Rockland Immunochemicals (Gilbertsville, PA), respectively.

Immunoprecipitation from rat tissues

Crude membrane fractions were prepared from adult rat brain, cerebral cortex, cerebellum, hypothalamus, and spinal cord (Pel-Freez Biologicals, Rogers, AR) or from freshly prepared neonatal cortex and cerebellum using a glass-Teflon tissue homogenizer and buffer A (320 mM sucrose, 5 mM HEPES, pH 7.4). Complete Protease Inhibitor Cocktail (Roche Diagnostics, Indianapolis, IN) was included in all buffer solutions used for protein preparation. Following centrifugation at 600 × g for 15 min post nuclear supernatant was centrifuged at 100,000 × g (30 min). The resulting membrane pellet was solubilized for 1 h in buffer B (100 mM NaCl, 40 mM KCl, 1 mM EDTA, 10% glycerol, 1% CHAPS, 20 mM HEPES, pH 7.4) and centrifuged at 50,000 × g for 30 min. The supernatant was incubated with $K_{2P}2.1$ antibody (mixture of C-20 and E-19) or control goat IgG (Sigma) overnight. Immune complexes were isolated with Protein G Sepharose (GE Healthcare), washed with buffer C (300 mM NaCl, 40 mM KCl, 1 mM EDTA, 0.5% CHAPS, 20 mM HEPES, pH 7.4), eluted with dithiothreitol (DTT)-containing SDS-PAGE sample buffer and subjected to Western blot analysis.

Cell culture

Transformed African Green Monkey kidney fibroblast (COS-7) and Chinese Hamster ovary (CHO) cells were cultured in DMEM and alpha-MEM (Invitrogen), respectively, supplemented with 10% fetal bovine serum, 2 mM L-glutamine, 100,000 U/l penicillin, and 100 mg/l streptomycin, and held at 37°C in humidified air with 5% CO_2. Cells were obtained from American Type Culture Collection (Manassas, VA) and the media and supplements were purchased from Invitrogen. Hippocampal neurons were prepared from embryonic day 18 (E18) Sprague Dawley rats as described (Marks et al., 2005). Dissociated cells were seeded on poly-L-lysine coated glass cover slips and maintained in NEURObasal media with 2% (v/v) B27 and 5 mM L-glutamine at 37°C in humidified air with 5% CO_2.

Protein expression and purification with COS-7 cells and *Xenopus* oocytes

cDNA encoding study proteins (18.75 μg cDNA/150 mm dish) was transiently expressed in COS-7 cells using LipofectAMINE 2000 (Invitrogen). One (Western blot, immunoprecipitation) or 10-20 plates (protein identification) were harvested 2 days after transfection. Oocytes were isolated from *Xenopus laevis* frogs (Nasco, Atkinson, WI) and treated with collagenase to ease removal of the follicular layer. cRNA encoding study proteins (15 ng/oocyte in 46 nl sterile water) was injected into 260 *Xenopus laevis* oocytes. After 2 days, oocytes were homogenized using a glass-Teflon tissue homogenizer. Protein extracts were prepared by solubilization in buffer B for 1 h and clarified by centrifugation at 50,000 × g for 30 min (COS-7 cell lysate) or 5,000 × g for 10 min (oocyte lysate). The resulting supernatant was either diluted with DTT-containing SDS-PAGE loading buffer and analyzed by Western blotting or subjected to immunoprecipitation. To perform immunoprecipitation using small scale preparations, the supernatant was incubated with $K_{2P}2.1$ antibody (T6448)

NIH-PA Author Manuscript

NIH-PA Author Manuscript

NIH-PA Author Manuscript

followed by isolation on Protein A Sepharose beads (GE Healthcare) and elution with DTT-containing SDS-PAGE loading buffer. For small and large scale preparations (protein identification), the supernatant was incubated with anti-1d4 IgG-coated Sepharose beads for 2 h. Unbound material was removed by washing with buffer C. Bound proteins were eluted with buffer D (100 mM NaCl, 40 mM KCl, 1 mM EDTA, 0.5% CHAPS, 1 mg/ml 1d4 peptide, 20 mM HEPES, pH 7.4) and diluted with DTT-containing SDS-PAGE loading buffer.

Protein identification

Large scale protein samples were analyzed by tandem electrospray ionization (ESI) liquid chromatography (LC) time-of-flight (TOF) mass spectrometry (MS) (ESI TOF LC-MS/MS; W.M. Keck Biotechnology Resource Laboratory), tandem ESI ion trap LC-MS/MS (Proteomics Core Lab, University of Chicago, IL) followed by NCBI database search using the Mascot algorithm, amino-terminal (Edman) sequencing (W.M. Keck Biotechnology Resource Laboratory), and Western blotting.

Western blot analyses

Lysates and eluates prepared in this study were subjected to SDS-PAGE on precast gels (Ready Gels, BioRad), prior to wet-transfer onto nitrocellulose paper and Western blot analyses using anti-rK_{2P}2.1 (CT68, 1:400-1:200), anti-rK_{2P}2.1 (CT26, 1:200), anti-rK_{2P}2.1 (T6448, 1:200) and anti-1d4 (1:5000). Secondary antibodies were used at 1:5000 dilutions. The secondary labeling of fluorescent conjugates was documented with an Odyssey scanner (Li-Cor Biosciences, Lincoln, NE), and quantitative analysis of labeling was performed with the Odyssey application software.

Surface expression assay for K_{2P}2.1

Oocytes were injected with cRNA encoding study proteins, as described above. For surface expression assays, cells were incubated with 0.7 mg/ml Sulfo-NHS-SS-Biotin (Pierce, Rockford, IL) for 2 h at room temperature prior to homogenization. Following biotinylation of lysine-exposing surface proteins, oocytes were rinsed and proteins were solubilized as described. Biotin-labeled proteins were isolated form oocyte lysate by incubation with Streptavidin beads (Pierce) for 1.5 h at 4°C and liberated by incubation with DTT-containing SDS-PAGE loading buffer.

Electrophysiology

For two-electrode voltage clamp (TEVC) recordings, defolliculated *Xenopus* oocytes were injected with 2-24 ng cRNA (depending on the experimental approach) encoding study channels in 23 nl of sterile water. Whole cell currents were measured 2 or 3 days after injection with an Oocyte Clamp amplifier (Warner Instruments, Hamden, CT) using pCLAMP9 (Axon Instruments, Foster City, CA) and Origin 6 (OriginLab, Northampton, MA) software for data acquisition and analysis. Data sampled at 2 kHz and filtered at 1 kHz. Electrodes filled with 3 M KCl and had tip resistances of 0.2-1 MΩ Recordings were performed under constant perfusion at room temperature. The standard, physiological extracellular solution was (in mM): 96 NaCl, 4 KCl, 1.1 $CaCl_2$, 1 $MgCl_2$, 5 HEPES (pH 7.4). All ionic changes were made by substitution with a chloride salt (RbCl, NH_4Cl, CsCl, LiCl) or N-methyl-D-glucamine (NMG) methanesulfonate. For recordings at 0-3 mM KCl, the extracellular NaCl concentration was 100 mM. At higher KCl concentrations, KCl was substituted for equimolar concentrations of NaCl. pH was adjusted to 7.4 where appropriate with NaOH, KOH, Tris or 2-[N-morpholino] ethanesulfonic acid (MeS). Currents evoked by step depolarization from -140 to +60 mV (500 ms) in 20 mV increments at 2 s intervals from the individually adjusted zero current holding potential (-80 mV for physiological solutions).

NIH-PA Author Manuscript

NIH-PA Author Manuscript

NIH-PA Author Manuscript

For inside-out patch-clamp studies, oocytes were injected with 12-24 ng cRNA and currents recorded 1-4 days after injection using an EPC-9 amplifier (HEKA Elektronik, Lambrecht, Germany). Data were stored on videotape. For off-line analysis, patch records were sampled at 20 kHz with pCLAMP9 software and digitally filtered at 2.8 kHz. Amplitude levels and open probabilities (assessed in single channel patches) were obtained by all-points histograms (0.05 pA bin size). Pipette and batch solutions contained 150 mM KCl, 1 mM EGTA, 10 mM HEPES (pH 7.4 with KOH). Recordings were performed at -60 or 60 mV holding potential.

Plasmid cDNAs (2 μg total channel cDNA or empty vector and 0.5 μg pEGFP/35 mm dish) were transfected into hippocampal neurons cultured for 7 days in vitro (DIV) using LipofectAMINE 2000 (Invitrogen) according to the manufacturer's instructions. Electrophysiological experiments were performed 24 to 48 h after transfection in a bath solution comprising 1.3 mM $CaCl_2$, 0.5 mM $MgCl_2$, 0.4 mM $MgSO_4$, 3.56 mM KCl, 0.44 mM KH_2PO_4, 139.7 mM NaCl, 0.34 mM Na_2HPO_4, 5.5 mM glucose, 10 mM HEPES (pH 7.4 with NaOH). Electrodes were fabricated from borosilicate glass (Clark, Kent, UK), coated with Sigmacote (Sigma) prior to use, and had a tip resistance of 3-5 MΩ when filled with a solution containing 136 mM KCl, 1 mM $MgCl_2$, 2 mM K_2ATP, 5 mM EGTA, 10 mM HEPES (pH 7.2 with KOH). Whole-cell patch clamp was performed as previously described (Plant et al., 2006) using an Axopatch 200B amplifier (Molecular Devices, Union City, CA) and pCLAMP9 software at filter and sampling frequencies of 5 and 25 kHz respectively for voltage-clamp experiments and 1 and 10 kHz respectively for current-clamp recordings. Linear changes in membrane potential either side of resting value were used to calculate the input resistance. Voltage-clamp errors were minimized with 80% series resistance compensation. Liquid junction potentials were measured on the Axopatch 200B at room temperature according to a method (Neher, 1992). Briefly, the patch electrode and recording chamber were filled with ND96 solution and voltage errors were corrected. Liquid junction potentials were determined for each test solution by perfusion into the recording chamber and measured as the offset required to maintain a zero current potential in I = 0 mode followed by a reperfusion test with ND96 to confirm the reversibility of each offset potential within 1 mV; measured values are in Table S3. Currents were elicited by step depolarization from -120 to +60 mV (500 ms) in 20 mV steps every 2 s (holding potential, -80 mV).

Live cell imaging

cDNA (1.5 μg cDNA per subunit type/35 mm dish along with an equal concentration of empty vector) transiently expressed in CHO cells grown on glass coverslips using LipofectAMINE 2000 (Invitrogen). Cells were analyzed 1 day after transfection. Fluorescence imaging of live cells performed by Metamorph software (Molecular Devices, Downington, PA) and an automated Olympus IX81 fluorescence microscope (Center Valley, PA). Images captured using a CCD camera and analyzed offline with ImageJ software (NIH).

Statistical analyses

Statistical significance assessed with Student's *t* tests using Origin 6.1 software (OriginLab, Northampton, MA). Multiple comparisons were performed using one-way ANOVA followed by Bonferroni *post hoc* testing.

Supplementary Material

Refer to Web version on PubMed Central for supplementary material.

NIH-PA Author Manuscript

NIH-PA Author Manuscript

NIH-PA Author Manuscript

Acknowledgements

This work was supported by a grant to S.A.N.G. from the National Institutes of Health and to D.T. from the Deutsche Forschungsgemeinschaft (TH1120/1-1). We are grateful to M.H. Butler, A. Kollewe, R. Goldstein and B. Thomas for discussion and advice during these studies. We thank S. Olikara and A. Sullivan for technical support.

References

Bockenhauer D, Zilberberg N, Goldstein SAN. KCNK2: reversible conversion of a hippocampal potassium leak into a voltage-dependent channel. Nature Neuroscience 2001;4:486–491.

Cai J, Huang Y, Li F, Li Y. Alteration of protein subcellular location and domain formation by alternative translational initiation. Proteins 2006;62:793–799. [PubMed: 16342262]

Doyle DA, Morais Cabral J, Pfuetzner RA, Kuo A, Gulbis JM, Cohen SL, Chait BT, MacKinnon R. The structure of the potassium channel: molecular basis of K+ conduction and selectivity. Science 1998;280:69–77. [PubMed: 9525859]

Duprat F, Lesage F, Patel AJ, Fink M, Romey G, Lazdunski M. The neuroprotective agent riluzole activates the two P domain K(+) channels TREK-1 and TRAAK. Mol Pharmacol 2000;57:906–912. [PubMed: 10779373]

Fernandez FR, Morales E, Rashid AJ, Dunn RJ, Turner RW. Inactivation of Kv3.3 Potassium Channels in Heterologous Expression Systems. J Biol Chem 2003;278:40890–40898. [PubMed: 12923191]

Fink M, Duprat F, Lesage F, Reyes R, Romey G, Heurteaux C, Lazdunski M. Cloning, functional expression and brain localization of a novel unconventional outward rectifier K+ channel. Embo J 1996;15:6854–6862. [PubMed: 9003761]

Galy B, Maret A, Prats A-C, Prats H. Cell Transformation Results in the Loss of the Density-dependent Translational Regulation of the Expression of Fibroblast Growth Factor 2 Isoforms. Cancer Res 1999;59:165–171. [PubMed: 9892202]

Goldstein SAN, Bayliss DA, Kim D, Lesage F, Plant LD, Rajan S. International Union of Pharmacology. LV. Nomenclature and Molecular Relationships of Two-P Potassium Channels. Pharmacol Rev 2005;57:527–540. [PubMed: 16382106]

Goldstein SAN, Bockenhauer D, O'Kelly I, Zilberberg N. Potassium leak channels and the KCNK family of two-P-domain subunits. Nature Reviews Neuroscience 2001;2:175–184.

Goldstein SAN, Price LA, Rosenthal DN, Pausch MH. ORK1, a potassium-selective leak channel with two pore domains cloned from Drosophila melanogaster by expression in Saccharomyces cerevisiae. Proc Natl Acad Sci 1996;93:13256–13261. [PubMed: 8917578]

Hann SR, King MW, Bentley DL, Anderson CW, Eisenman RN. A non-AUG translational initiation in c-myc exon 1 generates an N-terminally distinct protein whose synthesis is disrupted in Burkitt's lymphomas. Cell 1988;52:185. [PubMed: 3277717]

Heinemann U, Konnerth A, Pumain R, Wadman WJ. Extracellular calcium and potassium concentration changes in chronic epileptic brain tissue. Adv Neurol 1986;44:641–661. [PubMed: 3518350]

Heurteaux C, Lucas G, Guy N, El Yacoubi M, Thummler S, Peng X-D, Noble F, Blondeau N, Widmann C, Borsotto M, et al. Deletion of the background potassium channel TREK-1 results in a depression-resistant phenotype. Nat Neurosci 2006;9:1134. [PubMed: 16906152]

Honore E, Patel AJ, Chemin J, Suchyna T, Sachs F. Desensitization of mechano-gated K_{2P} channels. PNAS 2006;103:6859–6864. [PubMed: 16636285]

Ilan N, Goldstein SAN. KCNK0: single, cloned potassium leak channels are multi-ion pores. Biophysical Journal 2001;80:241–254. [PubMed: 11159398]

Kennard LE, Chumbley JR, Ranatunga KM, Armstrong SJ, Veale EL, Mathie A. Inhibition of the human two-pore domain potassium channel, TREK-1, by fluoxetine and its metabolite norfluoxetine. Br J Pharmacol 2005;144:821. [PubMed: 15685212]

Ketchum KA, Joiner WJ, Sellers AJ, Kaczmarek LK, Goldstein SAN. A new family of outwardly-rectifying potassium channel proteins with two pore domains in tandem. Nature 1995;376:690–695. [PubMed: 7651518]

NIH-PA Author Manuscript

NIH-PA Author Manuscript

NIH-PA Author Manuscript

Kevil C, Carter P, Hu B, DeBenedetti A. Translational enhancement of FGF-2 by eIF-4 factors, and alternate utilization of CUG and AUG codons for translation initiation. Oncogene 1995;11:2339–2348. [PubMed: 8570185]

Kindler CH, Yost CS, Gray AT. Local anesthetic inhibition of baseline potassium channels with two pore domains in tandem. Anesthesiology 1999;90:1092–1102. [PubMed: 10201682]

Kiss L, LoTurco J, Korn SJ. Contribution of the selectivity filter to inactivation in potassium channels. Biophysical Journal 1999;76:253–263. [PubMed: 9876139]

Kofuji P, Hofer M, Millen KJ, Millonig JH, Davidson N, Lester HA, Hatten ME. Functional analysis of the weaver mutant GIRK2 K+ channel and rescue of weaver granule cells. Neuron 1996;16:941–952. [PubMed: 8630252]

Korn SJ, Ikeda SR. Permeation selectivity by competition in a delayed rectifier potassium channel. Science 1995;269:410–412. [PubMed: 7618108]

Kozak M. An analysis of vertebrate mRNA sequences: intimations of translational control. J Cell Biol 1991;115:887–903. [PubMed: 1955461]

Kozak M. Initiation of translation in prokaryotes and eukaryotes. Gene 1999;234:187. [PubMed: 10395892]

Lopes CMB, Zilberberg N, Goldstein SAN. Block of Kcnk3 by Protons: evidence that 2-P-domain potassium channel subunits function as homodimers. J Biol Chem 2001;276:24449–24452. [PubMed: 11358956]

Lu B, Su Y, Das S, Liu J, Xia J, Ren D. The Neuronal Channel NALCN Contributes Resting Sodium Permeability and Is Required for Normal Respiratory Rhythm. Cell 2007;129:371. [PubMed: 17448995]

Lu NZ, Cidlowski JA. Translational Regulatory Mechanisms Generate N-Terminal Glucocorticoid Receptor Isoforms with Unique Transcriptional Target Genes. Molecular Cell 2005;18:331. [PubMed: 15866175]

Macri V, Proenza C, Agranovich E, Angoli D, Accili EA. Separable Gating Mechanisms in a Mammalian Pacemaker Channel. J Biol Chem 2002;277:35939–35946. [PubMed: 12121985]

Maingret F, Patel AJ, Lesage F, Lazdunski M, Honore E. Lysophospholipids open the two-pore domain mechano-gated K(+) channels TREK-1 and TRAAK. J Biol Chem 2000;275:10128–10133. [PubMed: 10744694]

Marks JD, Boriboun C, Wang J. Mitochondrial Nitric Oxide Mediates Decreased Vulnerability of Hippocampal Neurons from Immature Animals to NMDA. J Neurosci 2005;25:6561–6575. [PubMed: 16014717]

Mellentin JD, Smith SD, Cleary ML. lyl-1, a novel gene altered by chromosomal translocation in T cell leukemia, codes for a protein with a helix-loop-helix DNA binding motif. Cell 1989;58:77. [PubMed: 2752424]

Neher E. Correction for liquid junction potentials in patch clamp experiments. Methods Enzymology 1992;207:123–131.

Neyton J, Miller C. Discrete Ba2+ block as a probe of ion occupancy and pore structure in the high-conductance Ca2+ -activated K+ channel. Journal of General Physiology 1988a;92:569–586. [PubMed: 3235974]

Neyton J, Miller C. Potassium blocks barium permeation through a calcium-activated potassium channel. Journal of General Physiology 1988b;92:549–567. [PubMed: 3235973]

Noskov SY, Berneche S, Roux B. Control of ion selectivity in potassium channels by electrostatic and dynamic properties of carbonyl ligands. Nature 2004;431:830. [PubMed: 15483608]

Patel AJ, Honore E, Lesage F, Fink M, Romey G, Lazdunski M. Inhalational anesthetics activate two-pore-domain background K+ channels. Nat Neurosci 1999;2:422–426. [PubMed: 10321245]

Plant LD, Bowers PN, Liu Q, Morgan T, Zhang T, State MW, Chen W, Kittles RA, Goldstein SAN. A common cardiac sodium channel variant associated with sudden infant death in African Americans, SCN5A S1103Y. J Clin Invest 2006;116:430–435. [PubMed: 16453024]

Rhen T, Cidlowski JA. Antiinflammatory Action of Glucocorticoids -- New Mechanisms for Old Drugs. N Engl J Med 2005;353:1711–1723. [PubMed: 16236742]

NIH-PA Author Manuscript

NIH-PA Author Manuscript

NIH-PA Author Manuscript

Sánchez-Sánchez F, Ramírez-Castillejo C, Weekes DB, Beneyto M, Prieto F, Nájera C, Mittnacht S. Attenuation of disease phenotype through alternative translation initiation in low-penetrance retinoblastoma. Human Mutation. 200610.1002/humu.20394

Sesti F, Goldstein SAN. Single-channel characteristics of wildtype I_{Ks} channels and channels formed with two minK mutants that cause long QT syndrome. J Gen Phys 1998;112:651–664.

Shi N, Ye S, Alam A, Chen L, Jiang Y. Atomic structure of a Na+- and K+-conducting channel. Nature 2006;440:570. [PubMed: 16467789]

Shin N, Soh H, Chang S, Kim DH, Park C-S. Sodium Permeability of a Cloned Small-Conductance Calcium-Activated Potassium Channel. Biophys J 2005;89:3111–3119. [PubMed: 16143634]

Starkus JG, Kuschel L, Rayner MD, Heinemann SH. Ion Conduction through C-Type Inactivated Shaker Channels. J Gen Physiol 1997;110:539–550. [PubMed: 9348326]

Touriol C, Bornes S, Bonnal S, Audigier S, Prats H, Prats A-C, Vagner S. Generation of protein isoform diversity by alternative initiation of translation at non-AUG codons. Biology of the Cell 2003;95:169. [PubMed: 12867081]

Vagner S, Touriol C, Galy B, Audigier S, Gensac MC, Amalric F, Bayard F, Prats H, Prats AC. Translation of CUG- but not AUG-initiated forms of human fibroblast growth factor 2 is activated in transformed and stressed cells. J Cell Biol 1996;135:1391–1402. [PubMed: 8947560]

Wang Z, Zhang X, Fedida D. Regulation of transient Na+ conductance by intra- and extracellular K+ in the human delayed rectifier K+ channel Kv1.5. J Physiol 2000;523:575–591. [PubMed: 10718739]

Wollnik B, Schroeder BC, Kubisch C, Esperer HD, Wieacker P, Jentsch TJ. Pathophysiological mechanisms of dominant and recessive KVLQT1 K+ channel mutations found in inherited cardiac arrhythmias. Hum Mol Genet 1997;6:1943–1949. [PubMed: 9302275]

Zilberberg N, Ilan N, Goldstein SA. KCNKO: opening and closing the 2-P-domain potassium leak channel entails “C-type” gating of the outer pore. Neuron 2001;32:635–648. [PubMed: 11719204]

NIH-PA Author Manuscript
NIH-PA Author Manuscript
NIH-PA Author Manuscript

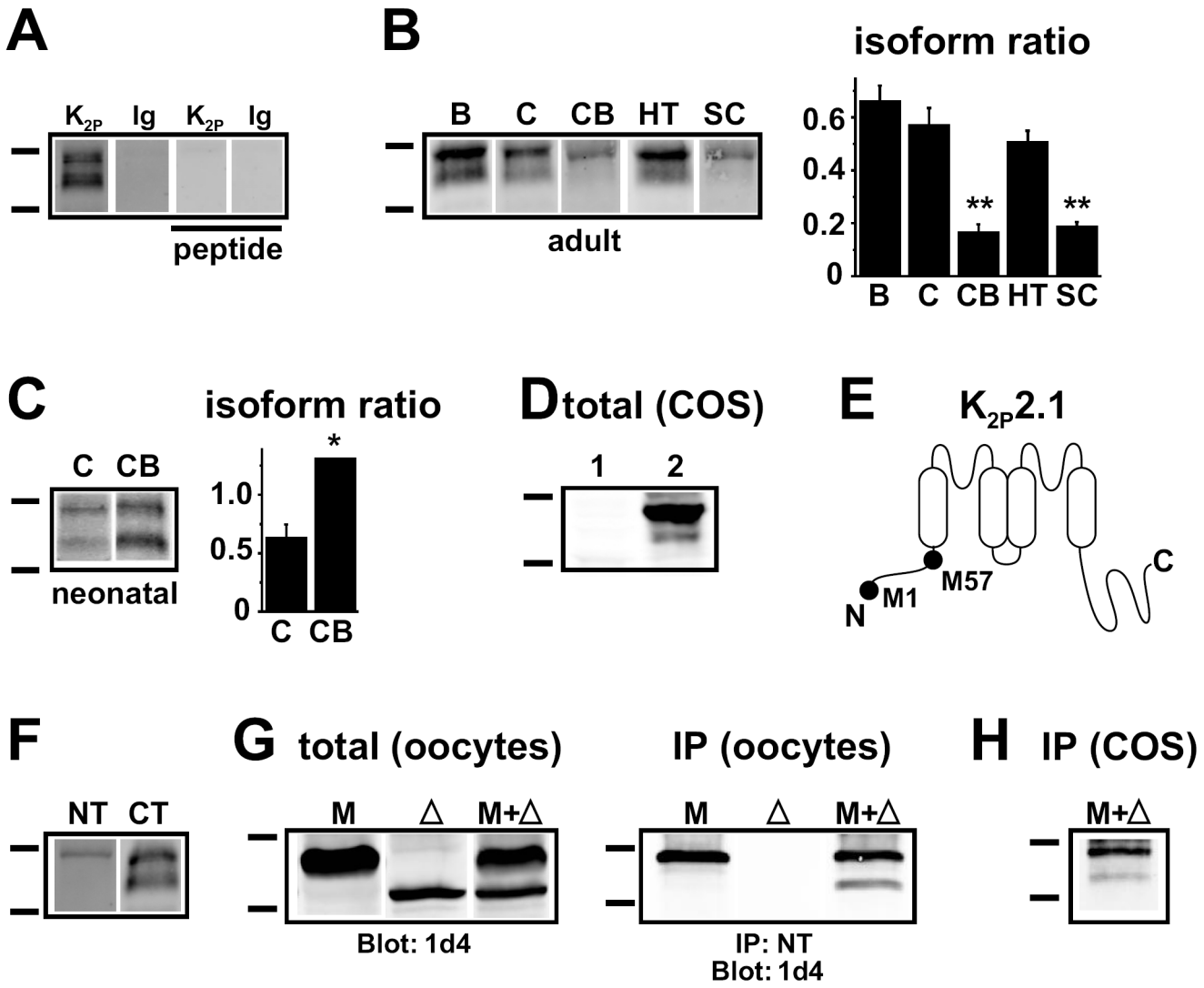

Figure 1. Two K_{2P}2.1 isoforms in rat brain and experimental cells

Full-length K_{2P}2.1 and Δ1-56 subunits are produced in rat central nervous system and experimental cells and form stable homomeric and mixed complexes. Markers correspond to apparent molecular weights: upper, 50 kDa; lower, 37 kDa.

(A) Isolation of two K_{2P}2.1 isoforms from rat brain membranes using a mixture of C-20 and E-19 antibodies directed against the C-terminus (K_{2P}) and control with non-specific IgG (Ig) as visualized by Western blot analysis with CT68, a third antibody to the K_{2P}2.1 C-terminus; specificity demonstrated by pre-treatment of CT68 with recombinant K_{2P}2.1 C-terminal peptide as indicated.

(B) K_{2P}2.1 isoform expression ratios by Western blot analysis as in panel a with CT68 antibody to the K_{2P}2.1 C-terminus in total adult rat brain (B), cerebral cortex (C), cerebellum (CB), hypothalamus (HT), and spinal cord (SC); plot is ratio of 41 / 47 kDa, mean ± SEM from 4-7 independent purifications; ** indicates difference from cortex ($p < 0.01$) whereas B and HT were not significantly different versus cortex ($p > 0.05$).

(C) K_{2P}2.1 variants isolated from neonatal rat brain and studied as described in panel a (C; cerebral cortex, CB; cerebellum). * indicates CB difference from C ($p < 0.05$).

NIH-PA Author Manuscript

NIH-PA Author Manuscript

NIH-PA Author Manuscript

(D) Western blot of COS-7 cells expressing empty vector (lane 1) or wild type human $K_{2P}2.1$ with an optimized initiation motif (lane 2) as in panel a with CT68 antibody to the C-terminus shows production of two $K_{2P}2.1$ isoforms.
(E) Topology of $K_{2P}2.1$ isoforms. Mass spectrometry and direct protein sequencing identify the two $K_{2P}2.1$ isoforms in COS-7 cells from the human gene to be full-length and Δ1-56 proteins, arising from translation initiation at positions M1 and M57, respectively (Figures S1 and S2A).
(f) $K_{2P}2.1$ protein isolated from rat brain and studied as described in panel a visualized with antibody to the channel N-terminus (NT; T6448) or C-terminus (CT; CT68).
(g) Western blot analysis of oocytes expressing M57I-1d4 (lane 1, **M**), truncated Δ1-56-1d4 (lane 2, Δ), or M57I-1d4 + Δ1-56-1d4 (lane 3, **M**+Δ). $K_{2P}2.1$ subunits visualized with anti-1d4 antibody. Left panel, total lysate; right panel, after immunoprecipitation with the N-terminal anti-$K_{2P}2.1$ antibody T6448 showing stable assembly of the two isoforms.
(h) IP lane demonstrates stable assembly of the two subunits in COS-7 cells by their co-immunoprecipitation with T6448 antibody to the N-terminus.

NIH-PA Author Manuscript
NIH-PA Author Manuscript
NIH-PA Author Manuscript

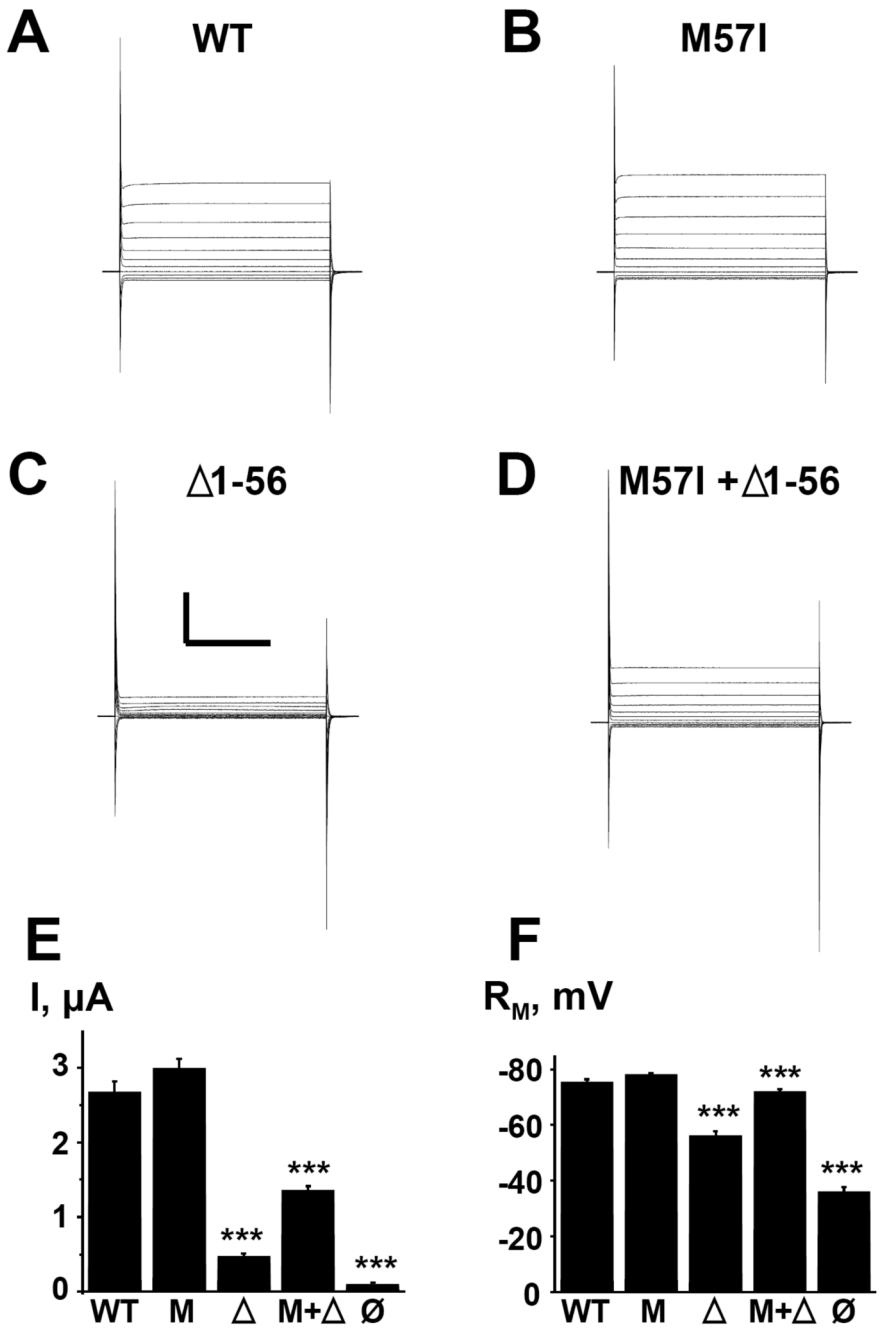

Figure 2. Δ1-56 yields small outward currents and membrane depolarization

Indicated subunits studied in *Xenopus* oocytes by two-electrode voltage clamp with physiological ionic conditions 3 days after injection of 2 ng total cRNA.

(A)-(D) Representative current families; scale bars, 4 μA and 200 ms.

(E) Mean outward currents at steady-state evoked by steps to 0 mV for groups of 21 cells injected with $K_{2P}2.1$ mRNA as follows: wild type (**WT**); M57I (**M**); Δ1-56 (lΔ); M57I + Δ1-56, 1 ng each (**M**+Δ); un-injected oocytes (**Ø**).

(F) Mean resting membrane potentials (R_M) of cells studied in panel e. ***$P < 0.001$ versus M57I; WT not different from M57I ($p > 0.05$). Error bars represent SEM.

NIH-PA Author Manuscript
NIH-PA Author Manuscript
NIH-PA Author Manuscript

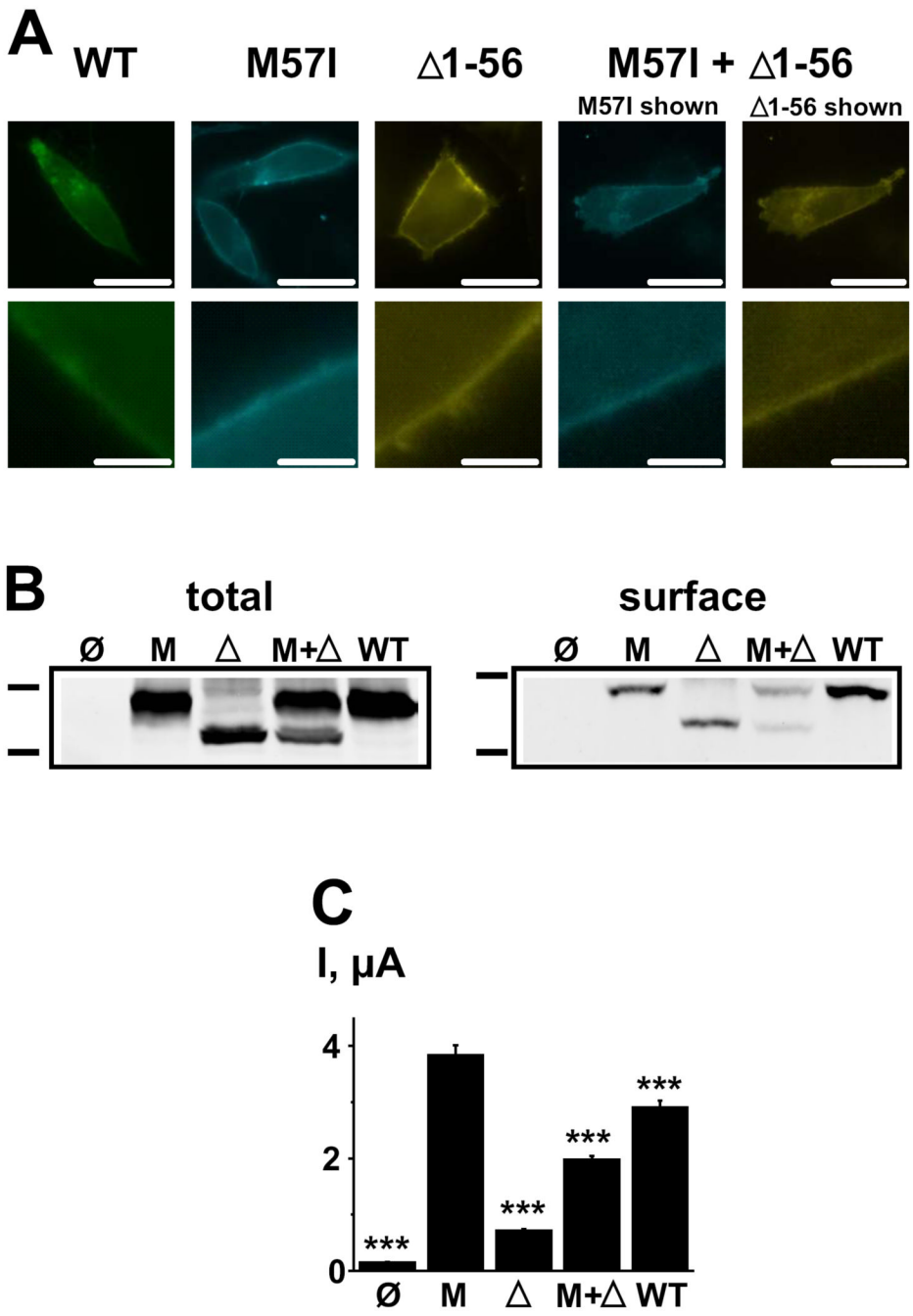

Figure 3. Δ1-56, M57I and heteromeric channels reach the plasma membrane

(A) Surface expression of WT-GFP, M57I-CFP, Δ1-56-YFP or mixtures in CHO cells with visualization by live cell microscopy. Scale bars, 20 μm (upper row) and 2 μm (lower).

(B) Western blot analysis of oocyte lysate (left) and surface protein isolated by biotinylation and purification on streptavidin beads (right), probed with anti-1d4 antibody and cells expressing: un-injected cells (lane 1, **Ø**); M57I-1d4 (lane 2, **M**); Δ1-56-1d4 (lane 3, Δ); M57I-1d4 + Δ1-56-1d4 (lane 4, **M**+Δ); WT-1d4 (lane 5, **WT**). Upper marker, 50 kDa; lower, 37 kDa. Three independent assays with similar results were performed.

(C) Mean (± SEM) outward currents evoked by depolarization to 0 mV (n = 12 cells each) for oocytes expressing channels indicated in panel b. ***$P < 0.001$ versus M57I.

NIH-PA Author Manuscript

NIH-PA Author Manuscript

NIH-PA Author Manuscript

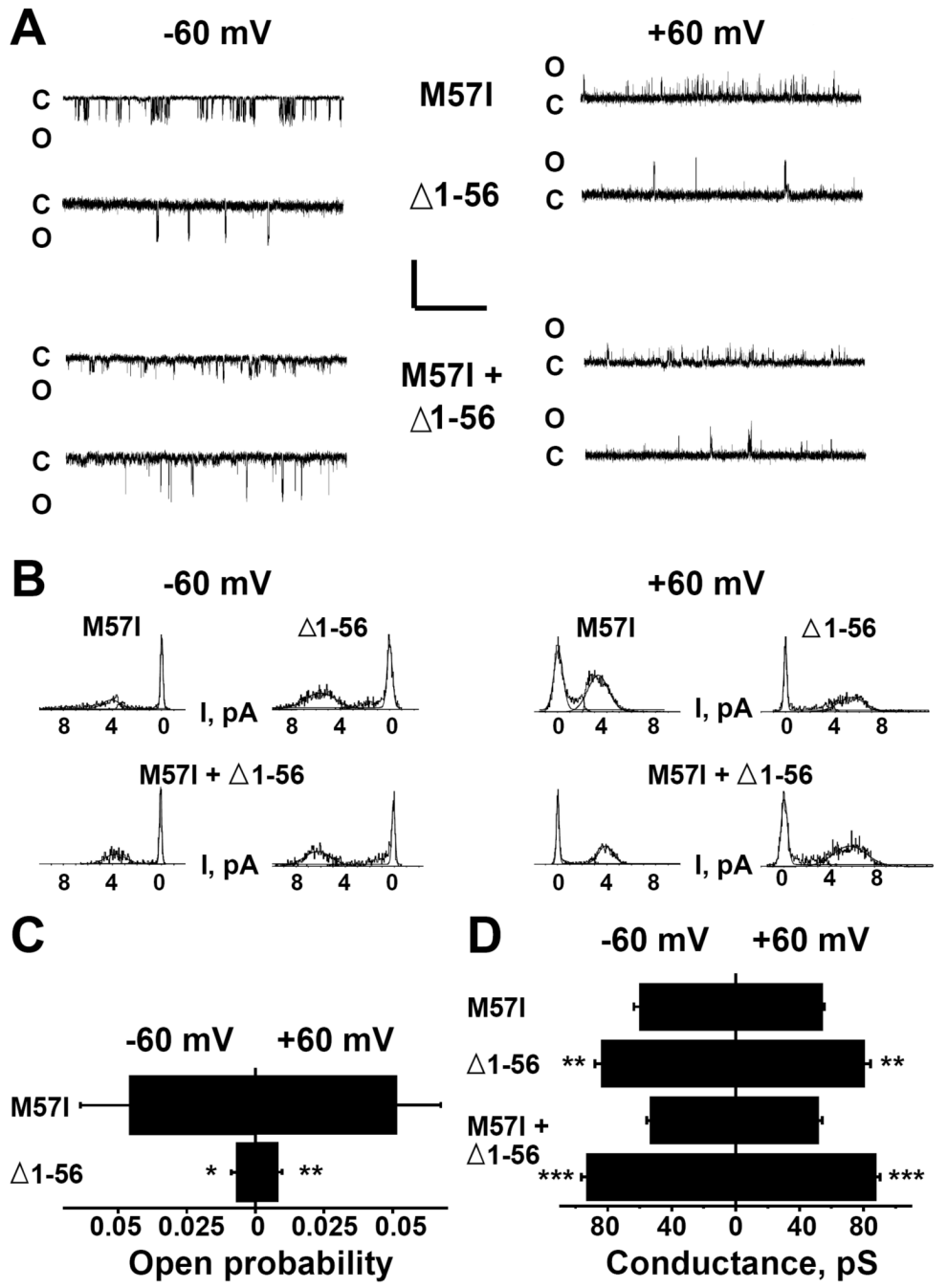

Figure 4. Δ1-56 channels have lower open probability and larger unitary conductance than M57I

Studies of indicated channels in patches excised from oocytes in inside-out mode with magnesium-free symmetric 150 mM KCl solution.

(A) Representative channel openings are shown at -60 or +60 mV with open (**O**) and closed (**C**) state levels indicated. Scale bars, 10 pA and 200 ms; sampled at 20 kHz, digitally filtered at 2.8 kHz.

(B) All-points histograms for openings at -60 mV (right) and +60 mV (left) of indicated subunits.

(C) Mean (± SEM) open probability (n = 3-9 single channel patches) were determined as indicated in Methods.

NIH-PA Author Manuscript

NIH-PA Author Manuscript

NIH-PA Author Manuscript

(D) Mean single channel conductances (± SEM) calculated from all-points histograms in symmetrical KCl at -60 and +60 mV (n = 5-14), were 60 ± 4 and 54 ± 1 pS for M57I channels and 83 ± 5 and 80 ± 4 pS for Δ1-56 channels, respectively. The two levels for subunit mixtures at -60 and +60 mV were 53 ± 3 and 93 ± 3 pS and 51 ± 3 and 87 ± 3 pS, respectively. **P* < 0.05, ***P* < 0.01, ****P* < 0.001 versus M57I.

NIH-PA Author Manuscript

NIH-PA Author Manuscript

NIH-PA Author Manuscript

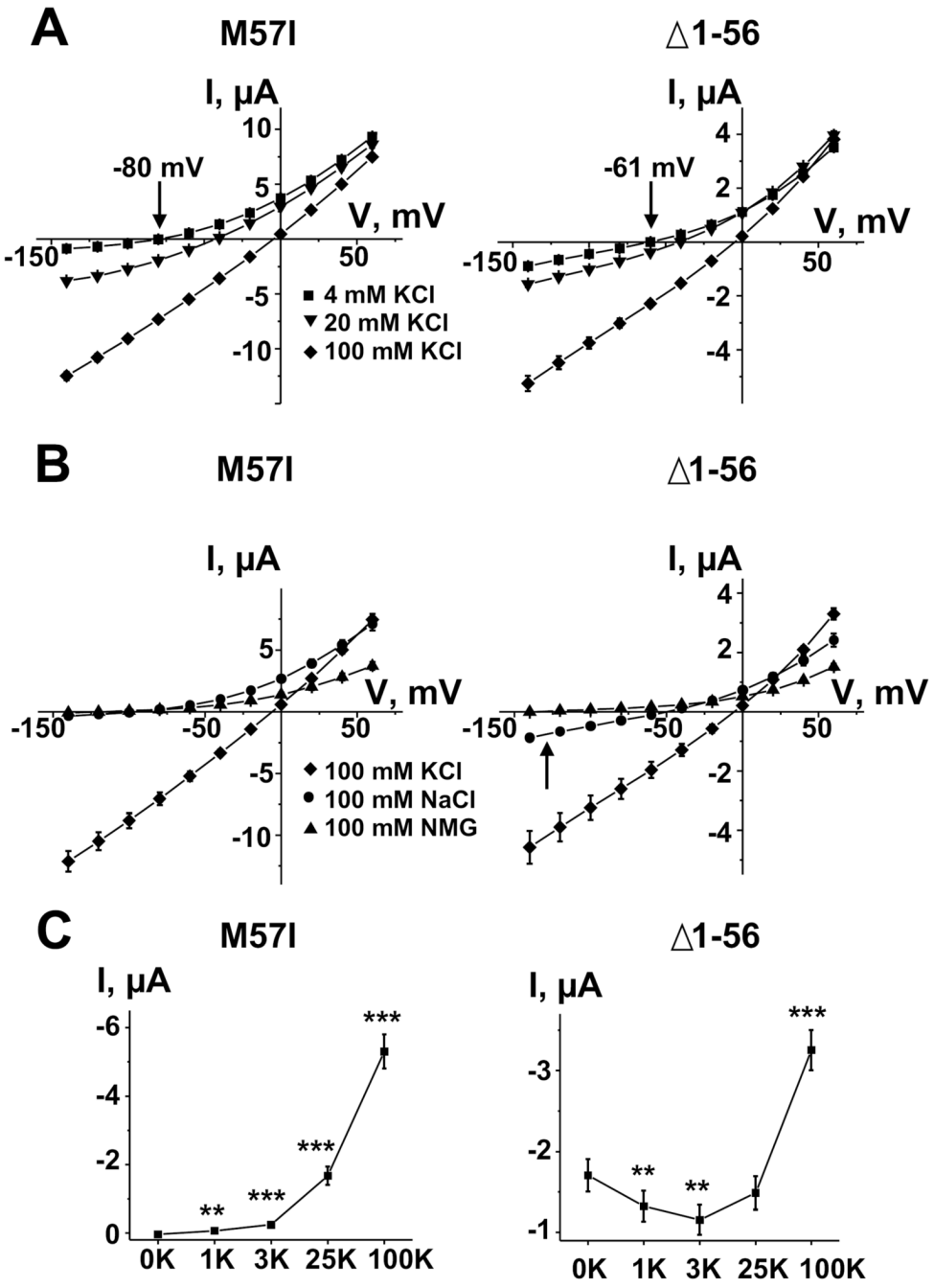

Figure 5. Δ1-56 channels pass sodium and show anomalous mole fraction behavior

Mean (± SEM) currents in oocytes expressing Δ1-56 or M57I channels as in Figure 2.

(A) Perfusion with 4 mM (squares), 20 mM (inverted triangles), and 100 mM KCl (diamonds), n = 16. Reversal potential in 4 mM KCl condition indicated by arrows.

(B) Perfusion with 100 mM KCl (diamonds), 100 mM NaCl (circles), or 100 mM NMG (triangles), n = 6. Arrow notes inward current with NaCl and no KCl in bath.

(C) Perfusion with various mole fractions of potassium and sodium (external KCl concentrations in mM). Plots show macroscopic inward current at -120 mV (mean ± SEM; n = 6-8. $^{**}P < 0.01$, $^{***}P < 0.001$ versus 0 mM KCl; Δ1-56 was not significantly different at 0

and 25 mM KCl ($p > 0.05$). At 0 to 3 mM KCl, extracellular NaCl was 100 mM. At higher concentrations, KCl was substituted isotonically for NaCl.

NIH-PA Author Manuscript
NIH-PA Author Manuscript
NIH-PA Author Manuscript

NIH-PA Author Manuscript

NIH-PA Author Manuscript

NIH-PA Author Manuscript

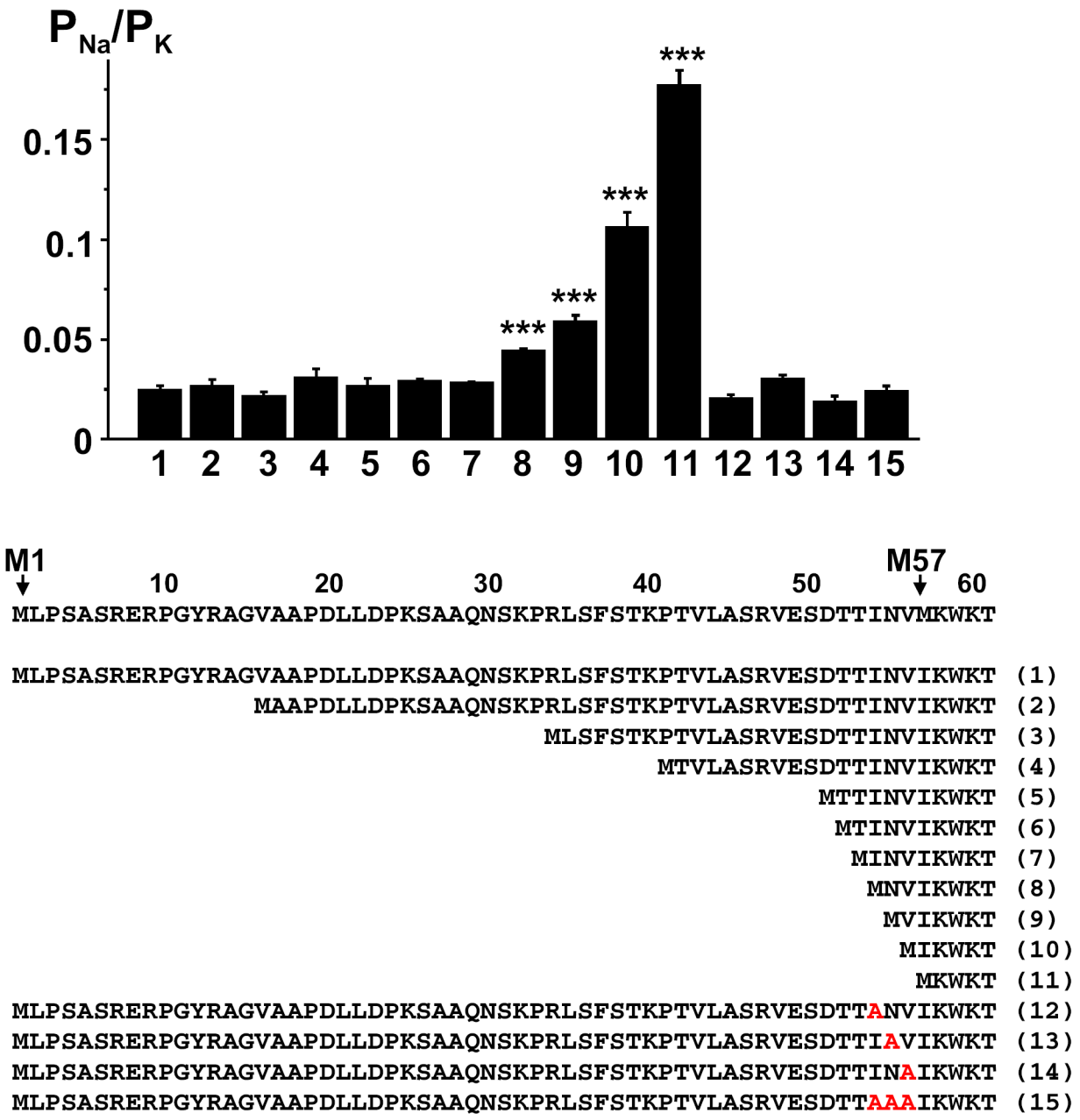

Figure 6. Molecular determinants of ion selectivity in K_{2P}2.1 variants

Relative permeability for sodium calculated from reversal potential measurements (P_{Na}/P_K; mean ± SEM; n = 10-33 cells) for various truncated K_{2P}2.1 channels indicated by number in the lower portion of the panel: 1, M57I; 2, Δ1-15/V16M-M57I; 3, Δ1-33/R34M-M57I; 4, Δ1-40/P41M-M57I; 5, Δ1-50/D51M-M57I; 6, Δ1-51/T52M-M57I; 7, Δ1-52/T53M-M57I; 8, Δ1-53/I54M-M57I; 9, Δ1-54/N55M-M57I; 10, Δ1-55/V56M-M57I; 11, Δ1-56; 12, I54A-M57I; 13, N55A-M57I; 14, V56A-M57I; 15, INV54-56AAA-M57I. ***P < 0.001 versus M57I; all other values were not significantly different from M57I.

NIH-PA Author Manuscript NIH-PA Author Manuscript NIH-PA Author Manuscript

Table 1

Macroscopic reversal potentials and monovalent cation selectivity of $K_{2P}2.1$ channels

Results expressed as permeability ratios (P_X/P_K; $P_K = 1$). Values represent mean ± SEM for n oocytes (voltage protocol in Experimental Methods). P_X/P_K was determined from whole cell reversal potential measurements where 100 mM KCl in the bath was replaced with the indicated cations according to the formula: $P_X/P_K = \exp(\Delta E_{rev}F/RT)$, where ΔE_{rev} is the reversal potential difference between the study ion and potassium, F is Faraday's constant, R is the gas constant, and T is temperature in degrees Kelvin, corrected offline for junction potential offsets as described in Experimental Methods.

channel		NaCl	KCl	RbCl	CsCl	LiCl	NH_4Cl
Δ1-56	E_{rev}(mV) P_X/P_K (n)	-48.2 ± 1.1 *** 0.177 ± 0.007 *** (20)	-2.8 ± 1.1 ^{NS} =1 (43)	1.1 ± 2.1 ** 0.669 ± 0.011 ^{NS} (7)	-51.9 ± 1.3 *** 0.083 ± 0.005 *** (7)	-49.3 ± 1.8 ** 0.095 ± 0.012 *** (7)	-17.5 ± 0.6 *** 0.326 ± 0.028 * (7)
M57I	E_{rev} (mV) P_X/P_K (n)	-99.2 + 2.2 0.024 ± 0.002 (24)	-2.4 ± 0.6 =1 (40)	-9.1 ± 1.5 0.627 ± 0.018 (6)	-72.7 ± 1.7 0.050 ± 0.002 (6)	-81.9 ± 3.4 0.037 ± 0.005 (6)	-35.2 ± 2.0 0.224 ± 0.017 (6)
Δ1-56 + M57I	E_{rev} (mV) P_X/P_K (n)	-77.6 ± 1.1 *** 0.056 ± 0.003 *** (18)	-2.9 ± 0.6 ^{NS} =1 (34)	-12.4 ± 1.1 ^{NS} 0.615 ± 0.011 ^{NS} (6)	-69.3 ± 1.1 ^{NS} 0.064 ± 0.003 ** (6)	-64.7 ± 3.2 ** 0.082 ± 0.012 ** (5)	-28.2 ± 1.0 * 0.310 ± 0.015 ** (4)
WT cRNA	E_{rev} (mV) P_X/P_K (n)	-100.2 ± 1.4 ^{NS} 0.022 ± 0.001 ^{NS} (16)	-2.4 ± 0.6 ^{NS} =1 (31)	-11.2 ± 1.1 ^{NS} 0.618 ± 0.013 ^{NS} (6)	-72.5 ± 0.7 ^{NS} 0.053 ± 0.001 ^{NS} (6)	-82.8 ± 0.9 ^{NS} 0.036 ± 0.001 ^{NS} (6)	-30.4 ± 0.8 * 0.283 ± 0.013 * (6)

* $P < 0.05$,

** $P < 0.01$,

*** $P < 0.001$ versus M57I;

^{NS} not significantly different from M57I ($p > 0.05$).

NIH-PA Author Manuscript
NIH-PA Author Manuscript
NIH-PA Author Manuscript

Table 2

Relative permeability for potassium and sodium in $K_{2P}2.1$ channels

Results expressed as relative permeability based on analysis in Table 1.

$K_{2P}2.1$ channel	Relative permeability for the indicated ion (P_K = 1)
Δ1-56	K^+ (1) > Rb^+ (0.67) > NH_4^+ (0.33) > **Na^+ (0.18)** > Li^+ (0.10) > Cs^+ (0.08)
M57I	K^+ (1) > Rb^+ (0.63) > NH_4^+ (0.22) > Cs^+ (0.05) > Li^+ (0.04) > **Na^+ (0.02)**
Δ1-56 + M57I	K^+ (1) > Rb^+ (0.62) > NH_4^+ (0.31) > Li^+ (0.08) > Cs^+ (0.06) ~ **Na^+ (0.06)**
WT cRNA	K^+ (1) > Rb^+ (0.62) > NH_4^+ (0.28) > Cs^+ (0.05) > Li^+ (0.04) > **Na^+ (0.02)**

NIH-PA Author Manuscript NIH-PA Author Manuscript NIH-PA Author Manuscript

Table 3

Biophysical Parameters for Hippocampal Neurons Transiently Expressing $K_{2P}2.1$ Channels

Neurons studied as described in Methods. R_M, resting membrane potential; R_{in}, input resistance (MΩ); $I_{0\ mV}$, peak current in voltage clamp (pA/pF) at 0 mV normalized to empty vector.

$K_{2P}2.1$ channel	Cells studied	R_M (mV)	R_{in}	$I_{0\ mV}$ (expt/cntl)
Δ1-56	9	-55.9 ± 1.0***	89.1 ± 1.1**	1.45 ± 0.04***
M57I	10	-75.4 ± 0.6	78.1 ± 1.5	2.71 ± 0.08
Δ1-56 + M57I	7	-71.0 ± 0.5**	79.0 ± 2.3*NS*	2.03 ± 0.25*
WT	4	-74.1 ± 0.7*NS*	81.4 ± 0.9*NS*	2.41 ± 0.12*NS*
Empty vector	10	-62.6 ± 0.7***	91.1 ± 1.0***	=1.0

*$P < 0.05$,

**$P < 0.01$,

***$P < 0.001$ versus M57I;

NS not significantly different from M57I ($p > 0.05$).